Shape from Mirrored Polarimetric Light Field

Shunsuke Nakagawa[1], Takahiro Okabe[3][a] and Ryo Kawahara[2][b]

[1]Department of Artificial Intelligence, Kyushu Institute of Technology, 680-4 Kawazu, Iizuka, Fukuoka 820-8502, Japan

[2]Graduate School of Informatics, Kyoto University, Yoshida-honmachi, Sakyo-ku, Kyoto, 606-8501, Japan

[3]Information Technology Track, Faculty of Engineering, Okayama University, 3-1-1 Tsushima-naka, Kita-ku, Okayama 700-8530, Japan

Keywords: 3D Shape Reconstruction, Polarization, Mirror.

Abstract: While mirror reflections provide valuable cues for vision tasks, recovering the shape of mirror-like objects remains challenging because they reflect their surroundings rather than displaying their own textures. A common approach involves placing reference objects and analyzing their reflected correspondences, but this often introduces depth ambiguity and relies on additional assumptions. In this paper, we propose a unified framework that integrates polarization and geometric transformations for shape estimation. We introduce a 9-dimensional polarized ray representation, extending the Plücker coordinate system to incorporate the polarization properties of light as defined by the plane of its electric field oscillation. This enables the seamless evaluation of polarized ray agreement within a homogeneous coordinate system. By analyzing the constraints of polarized rays before and after reflection, we derive a method for per-pixel shape estimation. Our experimental evaluations with synthetic and real images demonstrate the effectiveness of our method qualitatively and quantitatively.

1 INTRODUCTION

Recovering the shape of objects with perfectly mirror surfaces is challenging, as these objects reflect surrounding scenes rather than showing their inherent textures. The robust solution has a wide range of applications in product inspection, robotics, and extended reality (XR). Moreover, by leveraging the rich visual information reflected on the surface, the rays observable through a mirror contribute to wide-field-of-view shape recovery, precise localization, and efficient navigation.

In conventional studies, the shape cue of a mirrored object is extracted by placing a texture-referencing object, such as a display, and capturing its reflection with a camera. However, even if a correspondence is provided between the reference object and the camera, ambiguity about the object's shape remains because its depth is not uniquely determined. Therefore, assuming the surface integrability or leveraging the compound mirror's flatness is required for shape recovery (Takahashi et al., 2012).

Polarization provides a clue to resolving this ambiguity. The polarization before and after specular reflection varies depending on the surface normal of the object, allowing the normal to be recovered by utilizing multiple viewpoints (Miyazaki et al., 2012; Han et al., 2024) or the unique polarization pattern of the sky (Ichikawa et al., 2021). Lu *et al.* (Lu et al., 2019) proposed an approach to reconstructing complex mirror surfaces utilizing the polarization field generated by an LCD with one polarizing plate removed. However, it is necessary to use two or more calibrated polarized states of the liquid crystal, and the process additionally requires the extra step of attaching and detaching the polarizing plates.

In previous methods, the geometry of corresponding points and the constraints imposed by polarization are often treated independently or as separate steps. Additionally, in polarization-based methods, orthographic projection is typically assumed and recently extended to perspective projection models (Pistellato and Bergamasco, 2024). Can a framework be established that describes the geometric transformation of both within a unified analysis in 3D space? If achieved, this could naturally integrate the two modalities to provide a structured approach to analyzing solution spaces.

In this paper, we show that the geometrical transformation before and after reflection can be repre-

[a] https://orcid.org/0000-0002-2183-7112
[b] https://orcid.org/0000-0002-9819-3634

Nakagawa, S., Okabe, T. and Kawahara, R.
Shape from Mirrored Polarimetric Light Field.
DOI: 10.5220/0013389800003912

In *Proceedings of the 20th International Joint Conference on Computer Vision, Imaging and Computer Graphics Theory and Applications (VISIGRAPP 2025) - Volume 2: VISAPP*, pages 790-796
ISBN: 978-989-758-728-3; ISSN: 2184-4321

sented using a 9-dimensional polarized ray. Specifically, we extend the representation of light rays in the Plücker coordinate system by geometrically defining the properties of linearly polarized light as the normal to the oscillation plane of the electric field. Additionally, we derive constraints for shape estimation from the polarized rays before and after reflection. We enable a straightforward evaluation of the agreement between polarized rays by utilizing a homogeneous coordinate system, and we formulate shape recovery as a nonlinear optimization problem.

Our main contributions are as follows:

- Introducing the polarization light field, which extends the conventional light field by incorporating the plane of polarization normals and demonstrating that polarization rays can be handled through geometric transformations.
- Proposing a method for estimating the normal of a mirror surface object for each pixel by leveraging the reflection relationships of polarized rays.

2 RELATED WORK

Numerous studies have obtained the normal and position of the mirror surface from the reference point and its observation. In particular, in studies that focus on planar mirrors (Sturm and Bonfort, 2006; Rodrigues et al., 2010; Kumar et al., 2008), it is possible to recover the mirror surface even when the pose of the reference object is unknown. Takahashi *et al*. (Takahashi et al., 2012) leveraged multiple reflections to recover the normal of a multi-facet mirror from two or more corresponding points. On the other hand, since the normal of the curved mirror differs for each pixel, not only is a dense set of corresponding points required but also steps, such as moving the reference (Kutulakos and Steger, 2008; Grossberg and Nayar, 2005; Liu et al., 2011; Han et al., 2021), are required to obtain multiple constraints. Thus making it challenging to cover a wide range of objects' surfaces.

Some methods deal with the mirror surfaces by adding additional constraints, such as the integrability of the surface or radiometric clues (Liu et al., 2013; Chari and Sturm, 2013). There are methods that use LCDs as sources of polarized light (Lu et al., 2019; Kawahara et al., 2023). These techniques take advantage of polarization constraints through higher-order nonlinear optimization problems, and the geometric transformation relationships of polarization still require further exploration.

Shape from polarization (SfP), which reconstructs normals based on polarization, has been studied extensively for dielectric materials. Some SfP methods use specular reflection of unpolarized light as a clue for estimating the normal. However, there is ambiguity in the estimation (Atkinson and Hancock, 2006; Miyazaki et al., 2003), so SfP also leverages additional clues such as multi-view (Cui et al., 2017; Zhao et al., 2020) and shading(Smith et al., 2016; Huynh et al., 2010) and active lighting (Ma et al., 2007; Ichikawa et al., 2023).

While monocular SfP focuses on recovering surface normals, our approach geometrically unifies and analyzes both the dense feature point correspondences on the reference object and the polarization correspondences, enabling simultaneous depth recovery.

3 BASICS: POLARIZATION

Light is an electromagnetic wave that oscillates perpendicularly to the direction of propagation. The oscillation plane of light, invisible to the human eyes, has random directions for sunlight or incandescent lamps. This type of light is called unpolarized light. In contrast, light from LCDs and other sources that pass through linear polarizers has only a single oscillation plane, and this type of light is called linearly polarized light.

If we define a plane perpendicular to the direction of light propagation, the amplitude of the electric field of linearly polarized light can be represented as a 2D Jones vector $\check{e}$ as follows;

$$\check{e} = \begin{pmatrix} E_x \\ E_y \end{pmatrix} = \begin{pmatrix} E_0 \cos\alpha \\ E_0 \sin\alpha \end{pmatrix}, \tag{1}$$

where E_x and E_y are the x and y components of the amplitude E_0 in the plane.

We can leverage polarizing filters to obtain the angle α of the light oscillation in Eq. 1. A polarizing filter extracts the polarization component at a specific angle. Specifically, we place a polarizing filter in front of the camera and calculate the polarization angle α from the intensity captured at multiple known filter angles ψ. The amplitude transmission of the electric field $\check{e}_c(\psi)$ for a filter angle ψ can be described using the Jones calculus as follows (Collett, 2005);

$$\begin{aligned} \check{e}_c(\psi) &= \begin{pmatrix} \cos^2\psi & \cos\psi\sin\psi \\ \cos\psi\sin\psi & \sin^2\psi \end{pmatrix} \check{e} \\ &= E_0 \begin{pmatrix} \cos\psi\cos(\psi-\alpha) \\ \sin\psi\sin(\psi-\alpha) \end{pmatrix}. \end{aligned} \tag{2}$$

When the energy of this electric field is observed as intensity by a camera, the following holds;

$$I(\psi) \propto ||\check{e}_c(\psi)||_2^2. \tag{3}$$

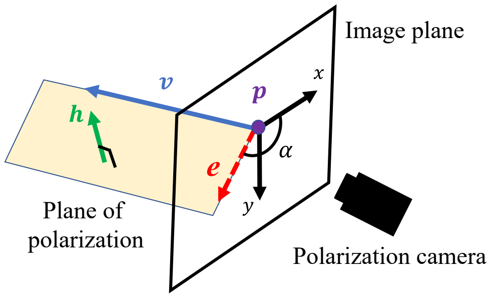

Figure 1: Polarized Ray. The plane of polarization is spanned by the direction of the electric field and the viewing direction.

Therefore, from Eq. 2 and Eq. 3, when the filter angle of the polarizing camera is ψ, linear polarization with AoLP α is observed with an intensity of

$$I(\psi) = I_0 + I_0 \cos(2\psi - 2\alpha). \tag{4}$$

We can utilize a quad-Bayer polarization camera to simultaneously obtain polarization images of four filter angles $\psi = (0, \pi/4, \pi/2, 3\pi/4)$ in a single shot and recover the sinusoidal in Eq. 4 (Huynh et al., 2010).

4 METHOD

By extending the existing light field representation, we describe the transformation of both polarization state and ray geometry and recover the shape of the mirror object by analyzing it.

4.1 Polarimetric Light Field

The viewing direction vectors for each pixel form a unique set of rays by mirror reflection. Let us describe the rays of the light field by extending them with polarization.

Polarized Ray. As shown in Fig. 1, The direction vector of the electric field at the image plane can be described in 3D space, using AoP α obtained from the observation as follows;

$$\boldsymbol{e} = \frac{1}{\sqrt{E_x^2 + E_y^2}} \begin{pmatrix} E_x \\ E_y \\ 0 \end{pmatrix} = \begin{pmatrix} \cos\alpha \\ \sin\alpha \\ 0 \end{pmatrix}. \tag{5}$$

The plane of polarization (PoP) on which the electric field oscillates is spanned by $\boldsymbol{e}$ and the viewing direction $\boldsymbol{v}_c$. Thus, we can represent PoP by its normal as

$$\boldsymbol{h} = \frac{\boldsymbol{v} \times \boldsymbol{e}^\top}{||\boldsymbol{v} \times \boldsymbol{e}^\top||} \tag{6}$$

Let us consider the expansion of the Plücker coordinates system (Sturm and Barreto, 2008) to evaluate whether rays are equivalent. This 6D homogeneous coordinate system can express arbitrary rays and consists of two components: the direction of the ray $\boldsymbol{v}$ and the normal δ of the plane spanned by the origin and the ray, also called the moment.

$$\begin{pmatrix} \boldsymbol{v} \\ \boldsymbol{\delta} \end{pmatrix} = \begin{pmatrix} \boldsymbol{v} \\ \boldsymbol{o} \times \boldsymbol{v} \end{pmatrix} \in \mathbb{R}^6, \tag{7}$$

where $\boldsymbol{o}$ denotes the origin of the ray, and $\boldsymbol{v}$ is a unit vector. We combine this with the PoP in Eq. 5 to define the polarized ray $\boldsymbol{\ell} \in \mathbb{R}^9$ as follows.

$$\boldsymbol{\ell} = \begin{pmatrix} \boldsymbol{v} \\ \boldsymbol{o} \times \boldsymbol{v} \\ \boldsymbol{h} \end{pmatrix}. \tag{8}$$

Note that there is a sign ambiguity in the normal vector that defines PoP.

Geometric Transformation. The coordinate transformation is linear w.r.t. the direction of the ray $\boldsymbol{\ell}$, the origin $\boldsymbol{o}$, and the PoP direction $\boldsymbol{h}$. Thus, the mirror transformation can be described using the Householder matrix H and the translation vector $\boldsymbol{t}_m$ as follows;

$$\begin{aligned} \boldsymbol{v}' &= H\boldsymbol{v}, \\ \boldsymbol{o}' &= H\boldsymbol{o} + \boldsymbol{t}_m \\ \boldsymbol{h}' &= H\boldsymbol{h}, \end{aligned} \tag{9}$$

where the H and $\boldsymbol{t}_m$ are defined by the mirror normal n and the distance to the mirror plane d_m as

$$H = I - 2\boldsymbol{n}\boldsymbol{n}^\top, \quad \boldsymbol{t}_m = -2d_m\boldsymbol{n}. \tag{10}$$

From Eq. 9, the mirror transformation of a polarized ray $\boldsymbol{\ell}$ can be described using a matrix $M \in \mathbb{R}^{9\times9}$, as follows;

$$\begin{aligned} \boldsymbol{\ell}' &= M\boldsymbol{\ell} \\ &= \begin{pmatrix} H & \boldsymbol{0} & \boldsymbol{0} \\ \boldsymbol{t}_m \times H & H & \boldsymbol{0} \\ \boldsymbol{0} & \boldsymbol{0} & H \end{pmatrix} \boldsymbol{\ell}. \end{aligned} \tag{11}$$

Up to this point, we can geometrically transform the polarized rays that consist of the polarized light field.

4.2 Shape from Mirrored Polarimetric Light Field

As shown in Fig. 2, suppose that the point $\boldsymbol{p}_d$ on the LCD is reflected on the object surface and observed in the polarization camera's viewing direction $\boldsymbol{v}_c$. The goal is to obtain the object surface's normal $\boldsymbol{n}$ and depth z. We first introduce the constraints for this imaging system when all the other unknowns are obtained.

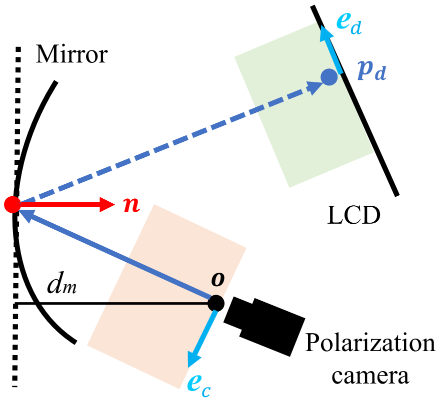

Figure 2: Shape from Mirrored Polarimetric Light Field.

Constraints. In summary, the constraint is that the mirror transformation of the polarized light observed by the camera matches the known polarized light defined on the display side. When the direction of the electric field $\boldsymbol{e}_c$ is obtained in the viewing $\boldsymbol{v}_c$ of the polarization camera, the PoP normal $\boldsymbol{h}_c$ is described as

$$\boldsymbol{h}_c = \frac{\boldsymbol{v}_c \times \boldsymbol{e}_c^\top}{||\boldsymbol{v}_c \times \boldsymbol{e}_c^\top||}. \tag{12}$$

Thus, the polarized ray ℓ_c obtained on the polarization camera side is described as

$$\ell_c = \begin{pmatrix} \boldsymbol{v}_c \\ \boldsymbol{o} \times \boldsymbol{v}_c \\ \boldsymbol{h}_c \end{pmatrix}, \tag{13}$$

where $\boldsymbol{o}$ is the camera's origin. Also, the polarized ray ℓ_c is reflected at the object surface to become ℓ_c' as

$$\ell_c' = M\ell_c = \begin{pmatrix} H\boldsymbol{v}_c \\ \boldsymbol{t}_m \times H\boldsymbol{v}_c \\ H\boldsymbol{h}_c \end{pmatrix}, \tag{14}$$

On the other hand, polarized light can also be described on the display side. When the corresponding point on the LCD is p_d and its electric field direction is e_d in the camera coordinate system, the PoP normal $\boldsymbol{h}_d$ is described as

$$\boldsymbol{h}_d = \frac{H\boldsymbol{v}_c \times \boldsymbol{e}_d^\top}{||H\boldsymbol{v}_c \times \boldsymbol{e}_d^\top||}. \tag{15}$$

Therefore, the polarized ray ℓ_d of the LCD side becomes

$$\ell_d = \begin{pmatrix} H\boldsymbol{v}_c \\ \boldsymbol{p}_d \times H\boldsymbol{v}_c \\ \boldsymbol{h}_d \end{pmatrix}. \tag{16}$$

Since these polarized rays are represented in homogeneous coordinates, ℓ_c' and ℓ_d become identical.

Noting the ambiguity of the sign of the PoP normal, we can obtain the constraints as

$$\begin{aligned} \boldsymbol{t}_m \times H\boldsymbol{v}_c - \boldsymbol{p}_d \times H\boldsymbol{v}_c &= \boldsymbol{0}, \\ H\boldsymbol{h}_c \times \boldsymbol{h}_d &= \boldsymbol{0}. \end{aligned} \tag{17}$$

The degree of freedom (DOF) of the normal n is 2, and the DOF of mirror plane distance d_m is 1, but Eq. 17 is nonlinear. Therefore, for robust estimation, we introduce regularization that assumes the integrability of the surface.

$$E_n = ||1 - \boldsymbol{n}^\top \boldsymbol{n}^+||_2^2, \tag{18}$$

where $\boldsymbol{n}^+$ is the surface normal calculated using the neighboring depth as

$$\boldsymbol{n}^+ = \frac{(-\partial_x z, -\partial_y z, 1)^\top}{||(-\partial_x z, -\partial_y z, 1)^\top||} \tag{19}$$

Note that the depth z can be obtained by the mirror plane distance d_m and z-component of the viewing z_{v_c} as $z = d_m z_{v_c}$. We define the following error function from Eq. 17 to optimize together with Eq. 18,

$$\begin{aligned} E_\delta &= ||(\boldsymbol{t}_m - \boldsymbol{p}_d) \times H\boldsymbol{v}_c||_2^2, \\ E_h &= ||H\boldsymbol{h}_c \times \boldsymbol{h}_d||_2^2. \end{aligned} \tag{20}$$

Finally, we consider the following minimization problem.

$$\min_{\boldsymbol{n}, d_m} (E_\delta + \lambda_h E_h + \lambda_n E_n), \tag{21}$$

where λ_h, λ_n are the optimization weight.

Shape Estimation. To obtain the direction of the electric field e_c from the polarization camera observations, we calculate the value of α in Eq. 4 for each pixel in the captured image, and then apply to Eq. 5. The direction of the electric field of the LCD is known as a product-specific angle in the image coordinate system of the LCD (typically, it is either horizontal, vertical, or $\pi/4$). Denoting the vector formed by applying this to Eq. 5 as $\hat{e}_d$, then e_d in the camera coordinate system is calculated with the calibrated display rotation R_d as

$$e_d = R_d \hat{e}_d. \tag{22}$$

Regarding the point p_d on the LCD corresponding to the camera's line of sight v_c, we leverage existing structured lighting to obtain the correspondence. Denoting the corresponding point in the LCD's local coordinate system as $\hat{p}_d$, the transformation to the camera coordinate system is described as

$$p_d = R_d \hat{p}_d + t_d, \tag{23}$$

where $\boldsymbol{t}_d$ is the translation vector of the display w.r.t. the camera. Up to this point, we have obtained the input for Eq. 21 to recover the shape through the optimization.

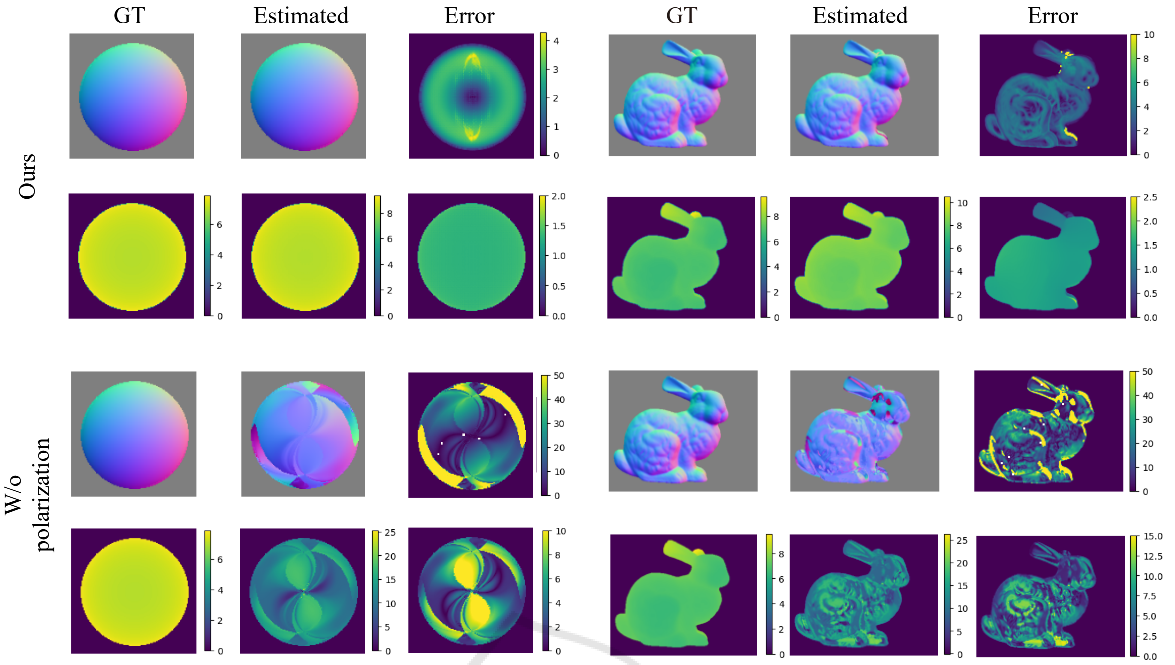

(a) (b)

Figure 3: The shape reconstruction results with synthetic (a) *Sphere* and (b) *Bunny* data. The upper row of each method shows the results of normal estimation, and the lower row shows the depth estimation results. The error maps of the normal are calculated as an angular error in degree, and the error maps of the depth are in cm.

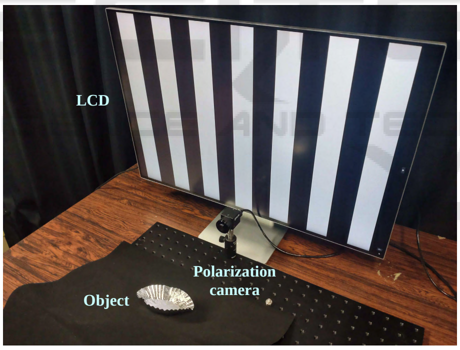

Figure 4: Experimental Setup.

5 RESULTS

In this section, we evaluate our method's prototyping and demonstrate its effectiveness through quantitative evaluation using synthetic data and reconstruction results using real images.

5.1 Quantitative Evaluation with Synthetic Data

We quantitatively evaluate the accuracy of our reconstruction using synthetic data. We rendered the simple-shaped *Sphere* and the complex-shaped *Bunny* as target objects under a linear polarized light source. Considering the actual environment, we set the distance from the camera to the object to be about 0.8 m and the size of the subject to be about 0.10 m. As a baseline method, we compare to the approach that does not utilize polarization (*i.e.* w/o E_h).

Here, the initial value of the normal vector is set to face the front, and the depth is set to 0.8 m as a plane. We used Pytorch's Adam optimizer for optimization and set $\lambda_h = 1.0$ and $\lambda_n = 100$ for Eq. 21. The number of iterations for parameter updates was set to 700. Regarding comparison methods, many SfP methods assume an unpolarized light source and dielectric material, which makes direct comparison difficult.

Fig. 3 shows the experimental results of the synthetic data. Although the shape obtained by our method was qualitatively accurate compared to the baseline method, an error can still be observed even in the experiment without the intensity noise. These results suggest that a local minimum exists in the optimization of Eq. 21. Specifically, the symmetric error structure shown in Fig. 3(a) suggests a local minimum that depends on the polarization direction of the display. This occurs when the optimization starts from the initial value of the normal vector that we set uniformly oriented forward.

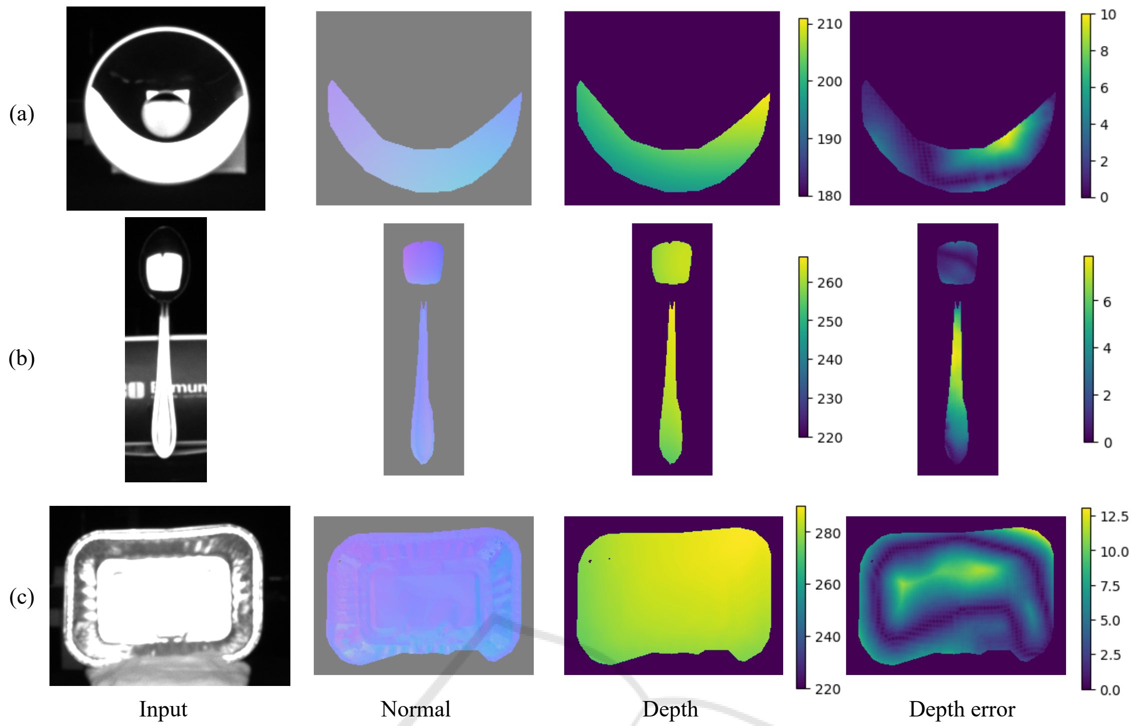

Figure 5: The shape reconstruction results of real-world objects. (a) *Elipse Mirror*, (b) *Spoon*, (c) *Aluminum cup*. The error of the depth map is in mm.

Table 1: Results of refractive index estimation.

Input	Error	**Ours**	w/o E_n	w/o E_h
Sphere	Normal (°)	0.74	0.87	8.15
	Depth (m)	0.042	0.047	0.167
Bunny	Normal (°)	2.62	2.99	13.31
	Depth (m)	0.106	0.124	0.316

5.2 Ablation Study

For further evaluation of the optimization, we verify the effect of the regularization term E_n through ablation experiments.

Table 1 shows the difference in results with and without the regularization term E_n and the PoP error cost E_h. These results show that the consistency of depth and normals work as effective guidance even for general shapes such as *Bunny* and that both normals and depth results are improved.

5.3 Real World Objects

As shown in Fig. 4, our system consist of a single LCD (HUAWEI MateView 3840×2560px) and a single polarization camera (FLIR BFS-U3-51S5P). The relative pose of the LCD and the polarization camera is calibrated beforehand using a planner mirror. We used the same strategy as in the simulation experiment in Sec. 5.1 for the initial normal and depth values. The ground truth depth value in the evaluation is obtained by aligning the depth camera (Intel RealSense D405) values.

Fig. 5 shows that our method can successfully recover the surface normals and depth of mirror objects in the real world. These results qualitatively demonstrate that both global and local shapes can be recovered. The average depth error are 2.84mm for *Elipse Mirror*, 3.21mm for *Spoon*, and 4.25mm for *Aluminum cup*, respectively. Note that the results only show the areas that can be recovered, and this area depends on the direction of the light source that the display can illuminate.

6 CONCLUSION

In this paper, we introduce a novel method for reconstructing the per-pixel surface normals and depths of mirror objects. By analyzing the polarization light field formed by polarized rays described in a homogeneous coordinate system, we clarify the geometric constraints imposed by both. Our approach unifies polarization and geometry under a single analysis, providing a structured and efficient method for reconstructing the shape of mirror surfaces. Experimental results show that our method can accurately reconstruct the per-pixel depths and surface normals of various mirror surfaces. Our future work includes extending the system to a polarized light source combining a mirror and LCD and calibrating a catadioptric system that handles polarization.

Limitations. The primary limitation of our method is that the reconstructible area of the object is limited by the spatial range of the display's illumination. This issue could be mitigated by using multiple LCDs or incorporating curved displays. Additionally, the method assumes a metallic surface, which may restrict its applicability. This limitation could be addressed by extending the approach to handle dielectric materials using Fresnel reflection.

ACKNOWLEDGEMENTS

This work was supported by JSPS KAKENHI Grant Numbers JP20H00612 and JP22K17914.

REFERENCES

Atkinson, G. A. and Hancock, E. R. (2006). Recovery of surface orientation from diffuse polarization. *IEEE TIP*, 15(6):1653–1664.

Chari, V. and Sturm, P. (2013). A theory of refractive photo-light-path triangulation. In *CVPR*, pages 1438–1445.

Collett, E. (2005). *Field guide to polarization*. Spie Bellingham.

Cui, Z., Gu, J., Shi, B., Tan, P., and Kautz, J. (2017). Polarimetric multi-view stereo. In *CVPR*, pages 1558–1567.

Grossberg, M. D. and Nayar, S. K. (2005). The raxel imaging model and ray-based calibration. *IJCV*, 61:119–137.

Han, K., Liu, M., Schnieders, D., and Wong, K.-Y. K. (2021). Fixed viewpoint mirror surface reconstruction under an uncalibrated camera. *IEEE TIP*.

Han, Y., Guo, H., Fukai, K., Santo, H., Shi, B., Okura, F., Ma, Z., and Jia, Y. (2024). Nersp: Neural 3d reconstruction for reflective objects with sparse polarized images. In *CVPR*, pages 11821–11830.

Huynh, C. P., Robles-Kelly, A., and Hancock, E. (2010). Shape and refractive index recovery from single-view polarisation images. In *CVPR*, pages 1229–1236.

Ichikawa, T., Nobuhara, S., and Nishino, K. (2023). Spiders: Structured polarization for invisible depth and reflectance sensing. *ArXiv*, abs/2312.04553.

Ichikawa, T., Purri, M., Kawahara, R., Nobuhara, S., Dana, K., and Nishino, K. (2021). Shape from sky: Polarimetric normal recovery under the sky. In *CVPR*, pages 14832–14841.

Kawahara, R., Kuo, M.-Y. J., and Okabe, T. (2023). Polarimetric underwater stereo. In *Scandinavian Conference on Image Analysis*, pages 534–550. Springer.

Kumar, R. K., Ilie, A., Frahm, J.-M., and Pollefeys, M. (2008). Simple calibration of non-overlapping cameras with a mirror. In *CVPR*, pages 1–7. IEEE.

Kutulakos, K. N. and Steger, E. (2008). A theory of refractive and specular 3d shape by light-path triangulation. *IJCV*, 76:13–29.

Liu, M., Hartley, R., and Salzmann, M. (2013). Mirror surface reconstruction from a single image. In *CVPR*.

Liu, M., Wong, K.-Y. K., Dai, Z., and Chen, Z. (2011). Specular surface recovery from reflections of a planar pattern undergoing an unknown pure translation. In *ACCV*, pages 137–147. Springer.

Lu, J., Ji, Y., Yu, J., and Ye, J. (2019). Mirror surface reconstruction using polarization field. In *ICCP*, pages 1–9.

Ma, W.-C., Hawkins, T., Peers, P., Chabert, C.-F., Weiss, M., Debevec, P. E., et al. (2007). Rapid acquisition of specular and diffuse normal maps from polarized spherical gradient illumination. *Rendering Techniques*, 9(10):2.

Miyazaki, D., Shigetomi, T., Baba, M., Furukawa, R., Hiura, S., and Asada, N. (2012). Polarization-based surface normal estimation of black specular objects from multiple viewpoints. In *2012 Second International Conference on 3D Imaging, Modeling, Processing, Visualization and Transmission*, pages 104–111.

Miyazaki, D., Tan, R. T., Hara, K., and Ikeuchi, K. (2003). Polarization-based inverse rendering from a single view. In *ICCV*, pages 982–982.

Pistellato, M. and Bergamasco, F. (2024). The raxel imaging model and ray-based calibration. *IJCV*, 132:4688—-4702.

Rodrigues, R., Barreto, J. P., and Nunes, U. (2010). Camera pose estimation using images of planar mirror reflections. In Daniilidis, K., Maragos, P., and Paragios, N., editors, *ECCV*, pages 382–395, Berlin, Heidelberg. Springer Berlin Heidelberg.

Smith, W. A., Ramamoorthi, R., and Tozza, S. (2016). Linear depth estimation from an uncalibrated, monocular polarisation image. In *ECCV*, pages 109–125. Springer.

Sturm, P. and Barreto, J. P. (2008). General imaging geometry for central catadioptric cameras. In *ECCV*, pages 609–622. Springer.

Sturm, P. and Bonfort, T. (2006). How to compute the pose of an object without a direct view? In *ACCV*, ACCV'06, page 21–31, Berlin, Heidelberg. Springer-Verlag.

Takahashi, K., Nobuhara, S., and Matsuyama, T. (2012). A new mirror-based extrinsic camera calibration using an orthogonality constraint. In *2012 IEEE Conference on Computer Vision and Pattern Recognition*, pages 1051–1058. IEEE.

Zhao, J., Monno, Y., and Okutomi, M. (2020). Polarimetric multi-view inverse rendering. In *ECCV*, pages 85–102. Springer.